Applied Surface Science 465 (2019) 154–163

Contents lists available at ScienceDirect

Applied Surface Science

journal homepage: www.elsevier.com/locate/apsusc

Full Length Article

Sol-gel synthesized hexagonal boron nitride/titania nanocomposites with enhanced photocatalytic activity

Yuanyuan Sheng[a], Jie Yang[a], Fang Wang[a], Lichun Liu[b], Hu Liu[c], Chao Yan[a,*], Zhanhu Guo[d,*]

[a] College of Material Science and Engineering, Jiangsu University of Science and Technology, Zhenjiang 212003, Jiangsu Province, China
[b] College of Biological, Chemical Sciences and Engineering, Jiaxing University, Jiaxing 314001, China
[c] National Engineering Research Center for Advanced Polymer Processing Technology, Zhengzhou University, Zhengzhou 450002, China
[d] Integrated Composites Laboratory (ICL), Department of Chemical & Biomolecular Engineering, University of Tennessee, Knoxville, TN 37934, USA

ARTICLE INFO

Keywords:
Hexagonal boron nitride
Sol-gel
Nanocomposite
Photocatalysis

ABSTRACT

Hexagonal boron nitride (H-BN)/titania (TiO_2) nanocomposites photocatalysts were synthesized by a facile sol-gel method. The structure was verified by comprehensive analysis from X-ray diffraction, Raman, X-ray photoelectron spectroscopy, Fourier transform infrared spectroscopy, scanning electron microscope and transmission electron microscope. The degradation of organic dyes such as rhodamine B (RhB) and methylene blue (MB) under UV light irradiation was used to measure the photocatalytic activity of the h-BN/TiO_2 nanocomposites. The photocatalytic performance and the stability of H-BN/TiO_2 nanocomposites in the degradation of dyes (MB and RhB) significantly outperformed pure TiO_2 nanoparticles. The formed B—O—Ti bond in H-BN/TiO_2 gave rise to a strong link between h-BN sheets and TiO_2 nanoparticles, and thus the charge transportation rate was improved and the recombination of electrons and holes was suppressed in the photocatalytic processes. The degradation percentage for RhB and MB reached 98% and 92% within 50 min irradiation. The degradation rate (k) of first-order linear value of h-BN/TiO_2 nanocomposites (0.05952 and 0.0498) for RhB and MB degradation was 3.64 and 4.22 times higher than that of pure TiO_2 (0.01637 and 0.0118). The enhanced photocatalytic property of the nanocomposites was attributed to the reduction in charge recombination and the adsorption interaction between organic dyes and h-BN. Consequently, h-BN sheets hold a great promise to enhance the photocatalytic activity of semiconductive materials.

1. Introduction

Semiconductor-based photocatalytic materials have great potential in environmental cleaning [1,2] and solar energy conversion [3,4]. It is becoming more and more attractive. However, there are still requirements for the preparation of more efficient photocatalysts nowadays. Due to its high photocatalytic activity, low cost and environmental friendliness, titanium dioxide (TiO_2) is one of the most efficient semiconductive photocatalysts. However, practical applications of TiO_2 were limited by its intrinsic defects, such as low quantum efficiency, low electronic properties and agglomeration of nanoparticles. In order to solve the problem of low efficiency of quantum efficiency and agglomeration, a lot of efforts have been applied to control the light catalyst crystal structure (such as crystallinity, the size of the nanoparticles and exposed surface [5–7]) and modify the surface (such as precious metals, carbon nanotube, graphene and other semiconductor materials [8–11]). The photogenerated electrons and holes induced by light irradiation recombine rapidly both in internal and on the surface of the semiconductor, limiting the effective participation in the catalytic process and resulting in a low total quantum efficiency for the photocatalysis [12–14]. The morphology of nanoparticles and the chemical composition including the phase of photocatalysts have also influenced the quantum efficiency [15]. At the same time, few studies [13,15] have concerned about the transfer of photogenerated electrons and holes, and the suppression of the electron-hole recombination. In order to improve the photocatalytic activity, especially the degradation of the interfacial hole oxidation and its derivatives, it is very important to study the recombination rate of holes and electrons transferred to the interface. In addition, the stability of photocatalysts, such as TiO_2, can be improved by decreasing the recombination rate of electrons and holes produced by light irradiation [16,17].

Two dimensional materials, such as graphene and MoS_2, can practically and significantly reduce the size of nanoparticles, prevent aggregation, inhibit recombination of electron and hole [18–21]. The

* Corresponding authors.
E-mail addresses: chaoyan@just.edu.cn (C. Yan), zguo10@utk.edu (Z. Guo).

https://doi.org/10.1016/j.apsusc.2018.09.137
Received 3 June 2018; Received in revised form 27 July 2018; Accepted 16 September 2018
Available online 20 September 2018
0169-4332/

study of TiO_2 based photocatalysts revealed that graphene could improve the photocatalytic efficiency of TiO_2 nanoparticles due to accelerated transfer rate of photogenic electrons [8,18,22]. Compared with graphene, hexagonal boron nitride (h-BN) sheets have similar characteristic structure and lattice parameters with graphene [23–25] and possess a higher specific surface area and better adsorption capacity of dyes [17,26,27]. Therefore, h-BN sheets could be a promising candidate for improving the photocatalytic efficiency of TiO_2. Each layer of h-BN is composed of boron and nitrogen atoms arranged alternately with in plane dimension direction forming six square grids. Each layer has sp^2 hybrid forms of B—N which are linked together by covalent bond. Van der Waals force exists between the layers. Recently, Fu et al. [17] found that the surface of h-BN could be naturally negatively charged by the ball milling and the h^+ could transfer from the activated ZnO to h-BN when they were brought into contact. Thus, the photocatalytic reduction ability of ZnO was improved. Two dimensional structures played an important role in improving the particle size, agglomeration, band gap and quantum efficiency, thus, the introduction of 2-D h-BN is helpful to improve TiO_2 nanoparticles photocatalytic properties.

In the present work, a photocatalytic nanocomposite of h-BN/TiO_2 was fabricated by using a facile sol-gel method. The prepared nanocomposites of h-BN/TiO_2 had a reduced particle size of TiO_2 and a fantastic combination between h-BN sheets and TiO_2 nanoparticles. The h-BN reduced the agglomeration of nanoparticles and enhanced the adsorption of dyes. For photocatalytic experiment, the UV absorption coefficient of dye solution was tested by UV spectrophotometer, and the first-order linear rate k was calculated. The photocatalytic mechanism of nano-composites was explored by photoluminescence (PL) and electrochemical impedance spectroscopy (EIS). The results demonstrated that the h-BN sheets can inhibit the recombination of charges, which in turn can improve the catalytic efficiency of the photocatalysts. To be noted, the stability of nanocomposites was also demonstrated to be consolidated by the introduction of h-BN sheets.

2. Experimental

2.1. Materials

Tetrabutyl titanate ($C_{16}H_{36}O_4Ti$, 98.0%, CP) was chosen as titanium precursor and purchased from Sinopharm Chemical Reagent Co., Ltd. Absolute ethyl alcohol (CH_3CH_2OH, AR) and acetic acid (CH_3COOH, AR) were obtained from Sinopharm Chemical ReagentCo., Ltd and used as received. The h-BN powders (99.9% metals basis, 1–2 μm) were purchased from Aladdin. Analytical grade methylene blue (MB), and rhodamine B (RhB) were purchased from Sinopharm Chemical Reagent Co., Ltd (manufactured by Shanghai Chemicals Co).

2.2. Preparation of h-BN/TiO_2 samples

2.2.1. Synthesis of titanium dioxide (TiO_2)

The typical synthetic process is as follows. 10 mL of tetrabutyl titanate was added to 20 mL of anhydrous ethanol and stirred with a magnetic stirrer for 30 min to prepare solution A. 20 mL of anhydrous ethanol was placed in a beaker, and then 2 mL of acetic acid was added under mechanical stirring. In addition, 1.5 mL of deionized water was dropped. In order to control the pH in the range of 2–3, concentrated hydrochloric acid was used and the obtained solution was marked as solution B. Then solution B was slowly dripped into Solution A (about 3 mL/min) under magnetic stirring. After magnetic stirring for 40 min, a white gel was obtained after continued stirring for another few minutes. The gel was dried in an oven under a constant temperature of 60 °C. The slightly yellowish product was finely ground in an agate mortar and calcined in a muffle furnace at 500 °C for 2.5 h, respectively. Finally, the samples were obtained after slowly cooling in the furnace.

2.2.2. Synthesis of h-BN/TiO_2 samples

A typical h-BN/TiO_2 sample was prepared by ultrasonically dispersing 0.15 g h-BN powder in 20 mL anhydrous ethanol for 2 days, followed by centrifugation with low speed (1000 rpm) to prepare solution A. 2 mL glacial acetic acid was then added into 20 mL anhydrous ethanol. Then 10 mL tetrabutyl titanate was added under magnetic stirring. A uniform mixture of precursor solution was obtained after stirring for another 30 min, as solution B. Solution B was dropwise added to the well-dispersed solution A (dripping rate is 4 mL/min). Hydrochloric acid was used to control the pH. After magnetic stirring for 5 h, a white emulsion was attained. Then the jelly was obtained after drying in oven under a constant temperature of 80 °C. The dried product was ground finely in an agate mortar and calcined in a muffle furnace at 500 °C for 2.5 h. Finally, specimens were obtained after cooling in the furnace. To evaluate the content of h-BN sheets, 10 mL solution A was taken, and weighed, then dried to obtain the concentration of h-BN sheets in the solution A. It was used to calculate the total mass of h-BN sheets in the nanocomposites.

2.3. Photocatalytic experiments

A homemade device containing two parts was used to test the photocatalytic performance. One part is an ultraviolet analyzer equipped with a UV light with a wavelength of 365 nm. Another part is a beaker containing 50 mL MB (1×10^{-5} M) or RhB ($1x10^{-5}$ M) solution and a certain amount of photocatalyst under a magnetic stirring. The distance between the UV light source and the surface of the reaction solution was set as ~9 cm. During the test, the prepared h-BN/TiO_2 sample (50 mg) was put into the prepared MB/RhB solution (50 mL). Before irradiation, the mixed solution was magnetically stirred in the dark for 30 min until the adsorption-desorption equilibrium between dye and photocatalyst was established. At a given time interval of 10 min, small amount of solution (5 mL) was taken out and centrifuged for 30 min at a speed of 8000 r/min. The concentration of residual MB/RhB in the solution as a function of irradiation time was analyzed using Lambert-Beer's law with a UV–Vis spectrophotometry. The feature absorption wavelength (λ = 552 nm for RhB and λ = 664 nm for MB) was selected to monitor their photocatalytic degradation. The degradation efficiencies were calculated by Eq. (1):

$$\eta = 1-\frac{c_t}{c_0} \times 100\% \quad (1)$$

where C_0 is the concentration of the reactant before illumination and C_t is the temporal concentration after irradiation for a desired time. As the absorbance of the solution is proportional to the concentration of the dyes, the ratio of C_t/C_0 is equal to the ratio of the absorbance (A_t/A_0). For comparison, the photocatalytic activity of pure TiO_2 nanoparticles and h-BN/TiO_2 nanocomposites was also tested using identical experimental conditions. After full degradation of dyes on the h-BN/TiO_2 nanocomposite was achieved by exposing the sample under UV light irradiation for 50 min, the recycling performance of the h-BN/TiO_2 nanocomposites was tested by a treatment of centrifugal separation, washing and drying for the nanocomposites and then another photocatalytic experiment as mentioned above. This process was repeated five times.

2.4. Characterization of h-BN/TiO_2

X-ray diffractometer (XRD-6000) with the Cu Kα radiation (λ = 0.15406 nm) operated at 40 kV and 30 mA at a 2θ range of 20–80° was used to observe the phase structure of the samples. Raman spectra were recorded using a micro-Raman spectrometer in the back scattering geometry with a 532 nm laser as the excitation source at room temperature. FTIR spectra of these samples were obtained to survey the bonds while the XPS to analyze the elemental composition on the Termo Scientifc ESCALab 250Xi using 200 W monochromated Al Kα

radiation. The surface morphologies and particle sizes were analyzed by a JEOL JEM-2010F transmission electron microscopy (TEM) under an accelerating voltage of 100 kV and a JSM-6480 scanning electron microscope (SEM), respectively. UV absorption spectra were obtained by using a scan UV–Vis spectrophotometer of UV-3600*. PL spectrum was measured at room temperature on an EDINBURGH INSTRUMENTS fluorescence spectrophotometer with the excitation wavelength at 315 nm. The electrochemical impedance spectroscopy (EIS) characterization was carried on the EG&G PARC M233 electrochemical workstation with three-electrode system. The samples were used as working electrode while platinum wire as counter electrodes and Ag/AgCl as the reference electrodes. 0.1 M K_2SO_4 as the electrolyte solution was used to conduct electrochemical experiment. EIS spectra were obtained under a perturbation potential of 10 mV with the frequency range of 100–10 mHz.

3. Results and discussion

The morphology of samples was investigated by AFM, SEM and TEM. The exfoliated h-BN nanosheets present the sizes ranging from tens to a few hundred nanometers and the thickness is less than 1 nm, as shown in Fig. 1a. Considering that the ideal thickness of single layer h-BN is 0.34 nm, the obtained h-BN nanosheets are about 1–3 layers. The SEM image also confirmed the layered structure of h-BN nanosheets (Fig. 1b). The prepared pure TiO_2 aggregated just similar to previous reports (Fig. 1c). While in the sample of the nanocomposites synthesized through the sol-gel method, TiO_2 nanoparticles displayed a uniform dispersion with a smaller size around 10 nm. TEM image (Fig. 1d)

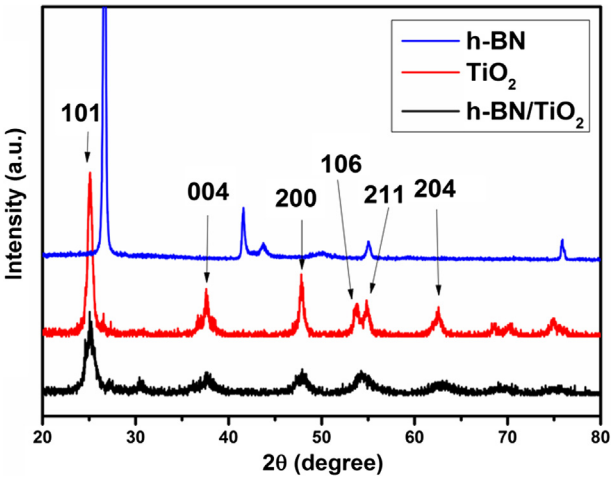

Fig. 2. XRD patterns of h-BN, the prepared h-BN/TiO_2 nanocomposites and pure TiO_2.

shows the structure of the h-BN/TiO_2 nanocomposites. The attachment of TiO_2 nanoparticles on the surface of h-BN sheets is observed. H-BN sheets have been integrated well with the TiO_2 nanoparticles. Selected area electron diffraction (SAED) was applied to reveal the crystal structure of the h-BN/TiO_2 nanocomposites, as shown in the inset of Fig. 1d. Based on the calculated value and analysis of diffraction patterns, diffractions can be indexed to the lattice plane of anatase TiO_2 (1 0 1), (0 0 4), (2 0 0), (1 0 5), (2 1 1) and the lattice plane of h-BN

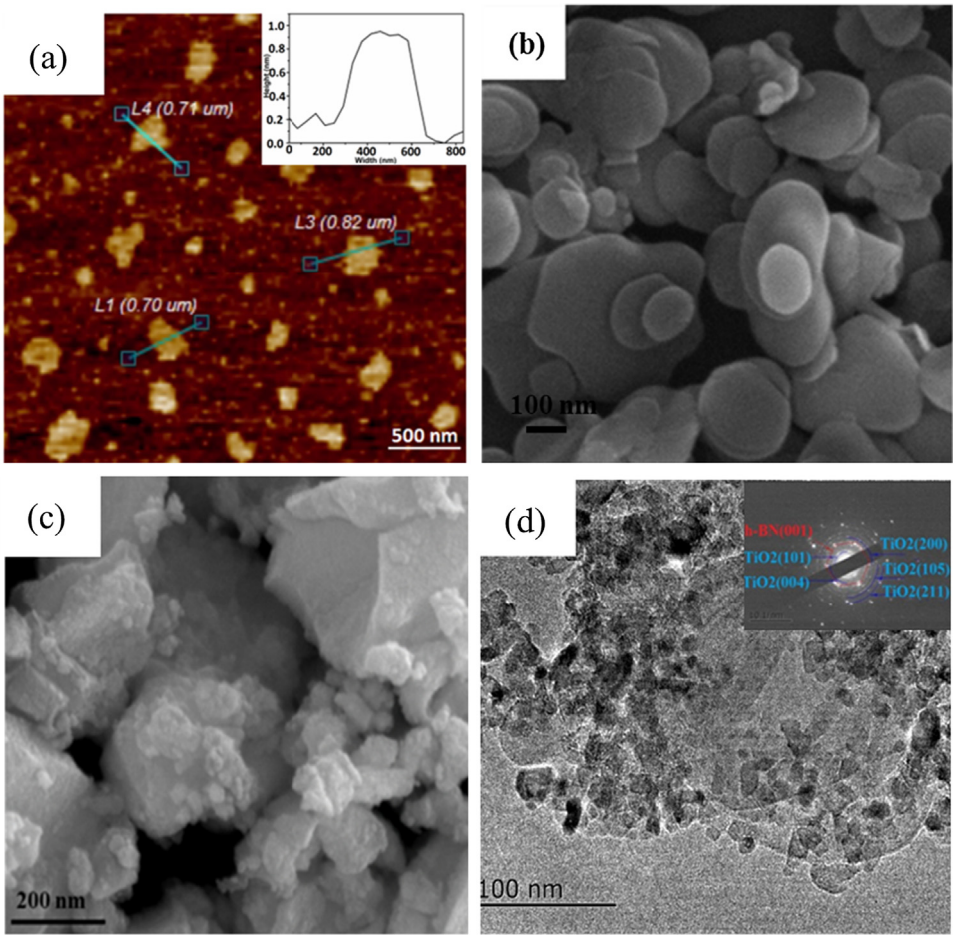

Fig. 1. (a) AFM image and height profile (inset) of bare h-BN, (b) SEM image of h-BN sheets, (c) TiO_2 nanoparticles and the (d) TEM image and ED pattern (the insert) of h-BN/TiO_2.

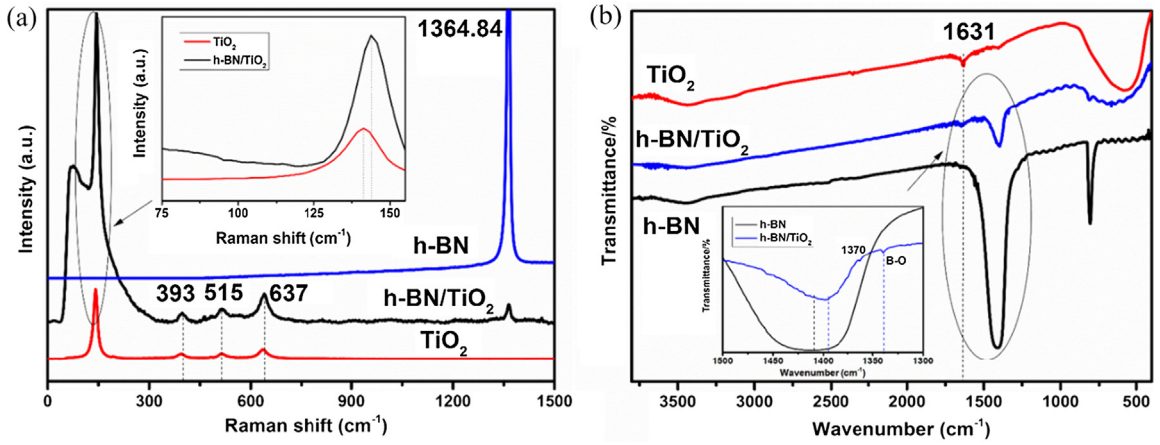

Fig. 3. (a) Raman spectra of h-BN, pure TiO_2 and h-BN/TiO_2 and magnified part (Insert), (b) FT-IR spectra of pure h-BN, TiO_2, h-BN/TiO_2 samples. (The inset details the B—N and B—O bonds).

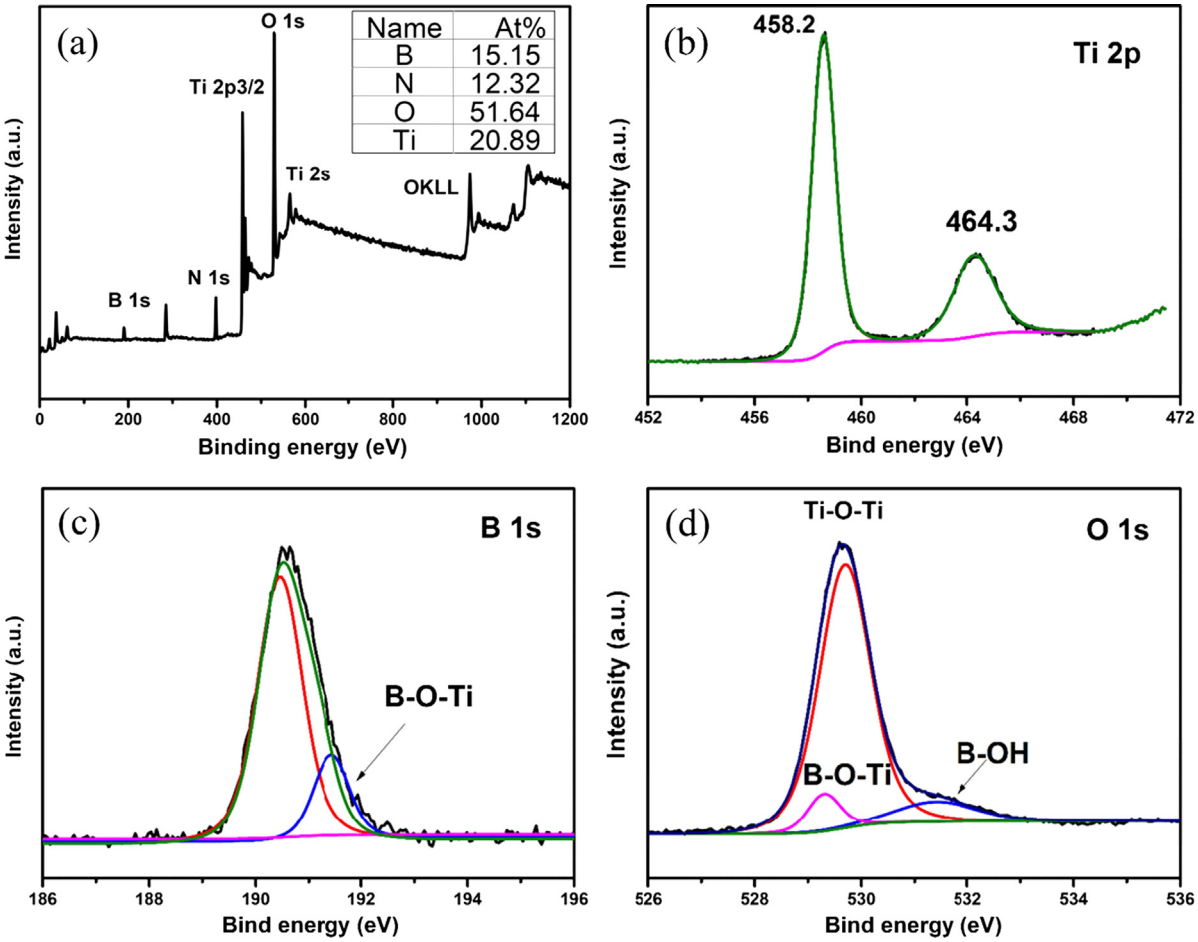

Fig. 4. XPS spectra of h-BN/TiO_2: (a) survey XPS spectrum, (b) high resolution Ti 2p, (c) B 1s, (d) O 1s.

(0 0 2), respectively [23,28].

The crystal structure was also characterized by X-ray diffraction (XRD). The diffraction of pure h-BN can be clearly observed at 26.7° (Fig. 2). The diffraction peaks located at 25.3, 37.9, 48.0, 54.4, 56.6, 62.8, and 68.9° can be indexed to (1 0 1), (0 0 4), (2 0 0), (1 0 5), (2 1 1), (2 0 4), and (1 1 6) plane of anatase TiO_2 [29,30], respectively. A weak diffraction peak (~26.7°) assigned to h-BN was observed in the h-BN/TiO_2 nanocomposites with strong diffractions of TiO_2. Furthermore, the calculated average anatase crystallite sizes of these particles using Scherrer's formula were 10.5 nm, which is smaller than that of pure TiO_2 of 11.6 nm. It is clearly shown that the TiO_2 particles supported on h-BN sheets were finer and more uniform than pure TiO_2. Smaller particle size contributed to the larger specific surface area, which improved the charge transportation and thus decreased the recombination probability of photoinduced electrons and holes [30].

Raman spectra of the samples were recorded in Fig. 3a. The typical Raman shift of the bare h-BN is located at 1364.84 cm^{-1} with strong intensity. The peaks around 144, 393, 515 and 637 cm^{-1} are identified to the anatase TiO_2 [31]. In the Raman spectrum of h-BN/TiO_2 nanocomposites, the present typical Raman shifts of both h-BN and anatase

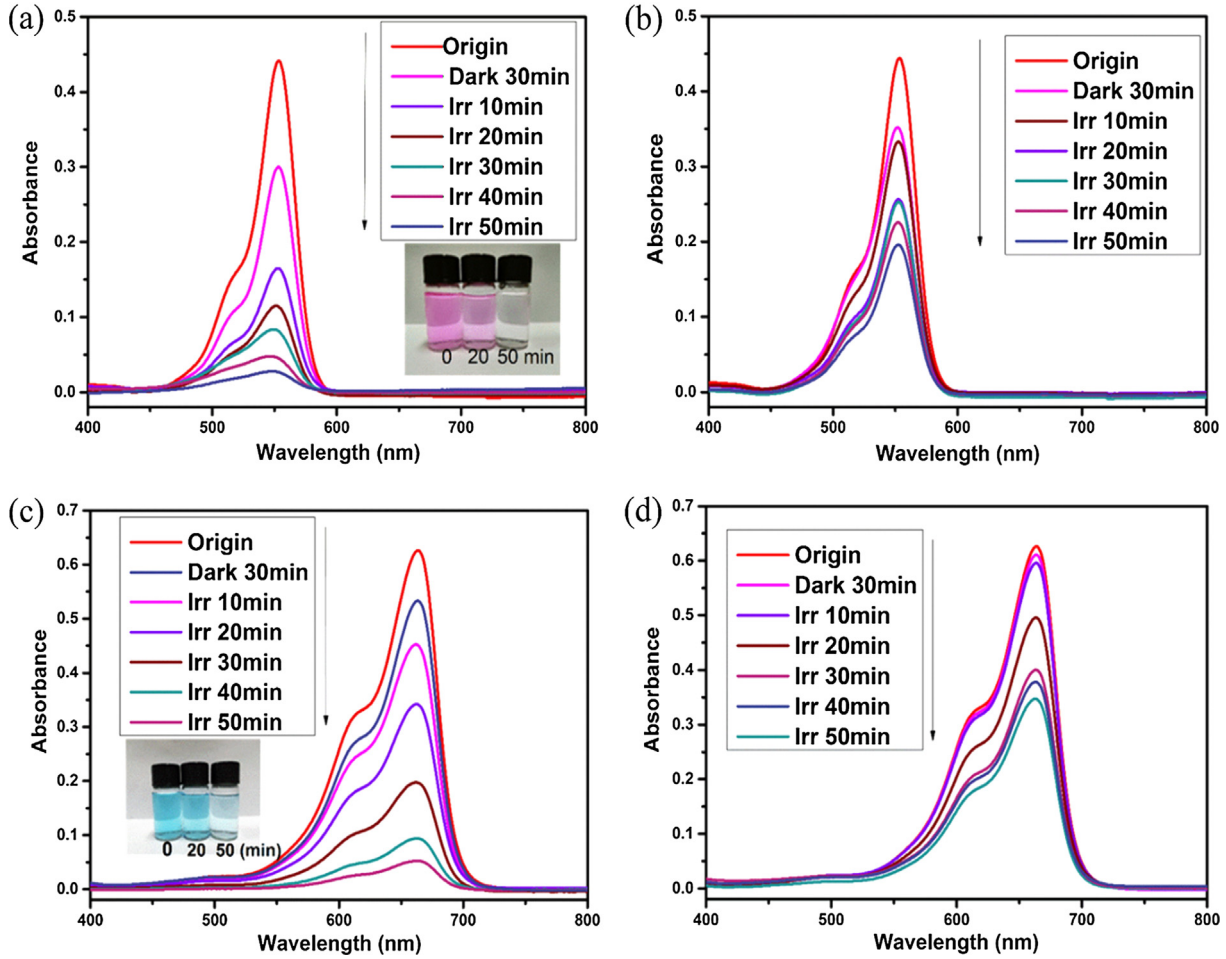

Fig. 5. UV–Vis absorbance spectra of dyes concentration with photocatalyst of (a) h-BN/TiO_2, (b) pure TiO_2 for RhB and (c) h-BN/TiO_2, (d) pure TiO_2 for MB.

TiO_2 are consistent with the XRD and SEAD results. TiO_2 does not undergo any phase transition upon the incorporation of h-BN sheets. Besides, compared to pure TiO_2, the peak at 144 cm^{-1} (Fig. 3a insert) of the h-BN/TiO_2 nanocomposites exhibits slightly blue shift and wider peak width, which are mainly affected by the size of nanoparticles and the oxygen vacancy defects [32]. The asymmetric broadening of the peak indicated a strong chemical interaction between TiO_2 nanoparticles and h-BN sheets [33,34]. In the FTIR spectra (Fig. 3b), the peak at 500–600 cm^{-1} corresponds to the Ti—O stretching vibration peak [33,34]. The broad band near 3400 and 1631 cm^{-1} was indexed to the stretching and bending vibration of hydroxyl groups, respectively. The peaks at 1408 and 806 cm^{-1} are attributed to the B-N stretching and bending modes of sp^2 hybridized BN skeletons, respectively. Interestingly, the exfoliated h-BN exhibits an obvious hydroxyl vibration near 3400 cm^{-1}. It evidently indicates that the hydroxyl groups are attached on the h-BN sheets after ultrasonic process, which is consistent with the previous reports [35]. The hydroxyl groups with negative charge on the h-BN sheets and the oxygen vacancies in TiO_2 nanoparticles could lead to a tight contact between h-BN sheets and TiO_2 nanoparticles. Moreover, the interaction between h-BN sheets and TiO_2 nanoparticles can also be evidenced by other two characteristics. One is the B—N peak of the h-BN/TiO_2 nanocomposites at 1390 cm^{-1} which shows slight shift compared to the exfoliated h-BN. The other is the present new peaks in the h-BN/TiO_2 nanocomposites located at around 1370 and 1331 cm^{-1} (Fig. 3b insert), which might be attributed to the B—O—Ti and the asymmetric B—O stretching vibration, respectively [33,34]. The X-ray photoelectron spectroscopy (XPS) measurement further confirmed the strong interaction between h-BN sheets and TiO_2 nanoparticles.

XPS measurement was carried out to elucidate the elemental composition and chemical states of h-BN/TiO_2, as shown in Fig. 4. The Ti_{2p} spectrum was composed of two individual peaks at 458.2 and 464.3 eV (Fig. 4b), which can be ascribed to the Ti $2p_{3/2}$ and Ti $2p_{1/2}$ binding energies, respectively. For the B 1s (Fig. 4c) spectrum, one main peak at 190.5 eV was attributed to B—N bonds while the other peak at 191.4 eV was assigned to the B—O—Ti bands [34,36]. As discussed above, bulk boron nitride was effectively exfoliated to a few layers and the hydroxyl groups were introduced. Due to the phonon effect and mechanical power, the defects of boron nitride and the exposure of B atoms made more active sites for further reactions [37]. In this work, the h-BN nanosheets were more favorable for the formation of B-O-Ti bands via the sol-gel method. And this was supported by the O 1s peak (Fig. 4d). The peak at 529.7 eV was attributed to the bonding of Ti—O—Ti [38], while the others with the binding energy centered at 529.1 and 531.4 eV belonged to the B—O—Ti and B—OH bonds, respectively [34,35,39–41]. The B 1s and N ls binding energies of the bulk h-BN are located at 190.18 and 399.08 eV (Fig. S1), respectively. Compared with reported the bulk h-BN, the B 1s and N1s spectrum of h-BN nanosheets upshifted 0.34 eV and downshifted 0.19 eV, respectively, which were caused by the introduction of hydroxyl group on the nanosheets after exfoliation. In the h-BN/TiO_2 nanocomposites, the center of B 1s binding energy is located at 190.64 eV because of the formation of B—O—Ti at 191.4 eV. The results suggested that h-BN nanosheets were bonded with TiO_2 nanoparticles very well, which is consistent with the Raman and Fourier FTIR results.

The photocatalytic activities of pure TiO_2 powder and h-BN/TiO_2 nanocomposites were measured by the decontamination of rhodamine b (RhB) and methylene blue (MB) dyes under UV light. Under

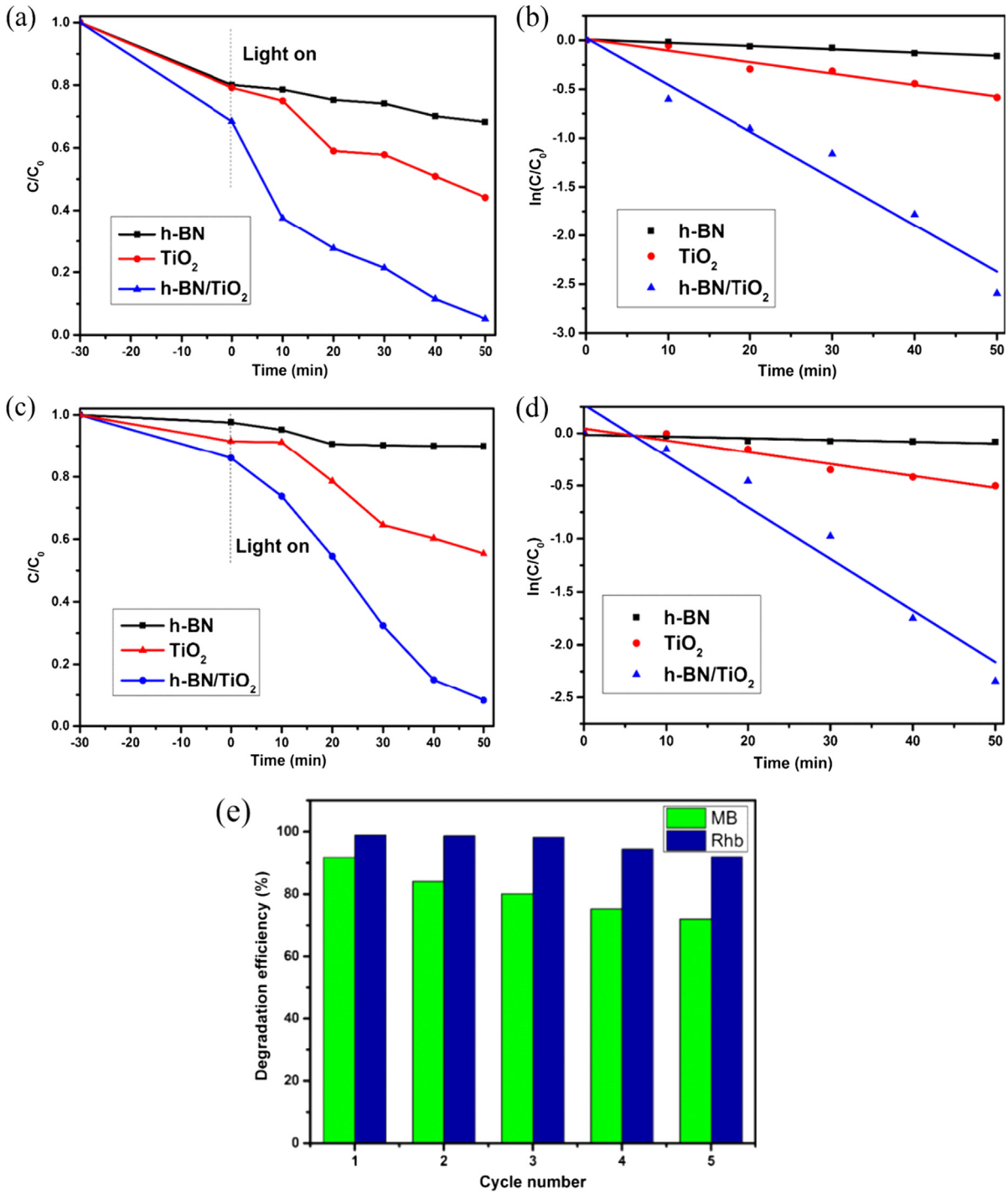

Fig. 6. Plots of C/C_0 and $\ln(C/C_0)$ versus time under UV light irradiation over different catalysts for RhB/MB. (a, b) RhB, (c, d) MB, (e) cycle runs of h-BN/TiO_2 nanocomposites photodegradation of RhB/MB dyes.

Table 1
Degradation rate (min^{-1}) constant k of prepared samples of h-BN/TiO_2, TiO_2, h-BN.

	Rhb	MB
h-BN	0.00765	0.0021
TiO_2	0.01637	0.0118
h-BN/TiO_2	0.05952	0.0498

irradiation, the TiO_2 were excited and the photo generated carriers could transfer to the nearby dye molecules and took part in the redox reactions, which led to the decomposition of dye into CO_2 and H_2O [30,35]. According to the UV–Vis absorbance spectra (Fig. 5), the h-BN/TiO_2 nanocomposites showed remarkable improvement on the photocatalytic performance. The RhB molecules were efficiently degraded using h-BN/TiO_2 nanocomposites within 50 min, which was much faster than that of pure TiO_2 nanoparticles (Fig. 5a and b). For the MB solution, h-BN/TiO_2 nanocomposites also exhibited a better performance, showing an obvious photocatalytic degradation within 50 min, whereas the decontamination effects were weak on pure TiO_2

Table 2
Recent studies on TiO_2 based photocatalysts and the corresponding application for organic decomposition.

Catalyst	Dosage (mg)	Dye	Concentration (Mg/L)	Volume (ml)	Light source	Irradiate time (min)	Removal rate (%)	article
TiO_2	50	AO7	10	50	500w Xenon lamp λ > 420 nm	60	5	[28]
N-TiO_2	50	AO7	10	50	500w Xenon lamp λ > 420 nm	60	8	[28]
N-TiO_2-RGO	50	AO7	10	50	500wc Xenon lamp λ > 420 nm	60	64.9	[28]
N.V-TiO_2-RGO	50	AO7	10	50	500w Xenon lamp λ > 420 nm	60	74.6	[28]
P25	30	MB	10	40	UV λ = 365 nm	60	68	[42]
P25-MWCNT-GR	30	MB	10	40	UV λ = 365 nm	60	73	[42]
P25-GR	30	MB	10	40	UV λ = 365 nm	60	96	[42]
S-TiO_2 (self-control)	40	RhB	10	40	500w Xenon lamp λ > 420 nm	120	39	[43]
TiO_2-Ag-5%	40	RhB	10	40	500w Xenon lamp λ > 420 nm	120	90	[43]
Nafion-GO		MO	11	2	UV	180	46	[44]
Nafion-TiO_2		MO	11	2	UV	180	67	[44]
120-rGO-TiO_2	10	MB	10	80	Solar light	300	80	[45]
150-rGO-TiO_2	10	MB	10	80	Solar light	300	98	[45]
180-rGO-TiO_2	10	MB	10	80	Solar light	300	100	[45]
h-BN/Ag_2CO_3		RhB			500w Xenon lamp λ > 420 nm	60	93	[46]
Milled h-BN/TiO_2	100	MB RhB	5.5	50	UV λ = 365 nm	30	98 98.5	[47]
Milled h-BN/ZnO	100	MB RhB	5.5	50	UV λ = 365 nm	25	60 82	[17]
Microwave TiO_2-graphene	50	MB RhB	5.5	100	UV λ = 310 nm	60	47.2 55.3	[48]
0.6TiO_2-RGO-C	30	MB	12	300	UV λ = 254 nm	Dark 180 Irradiate 180	90	[49]
P-TiO_2	100	RhB	10	40	150 W GYZ220 high-pressure Xenon lamp	150	98	[50]
h-BN/TiO_2	50	MB/RhB	5.5	50	UV λ = 365 nm	50	92 98	This work

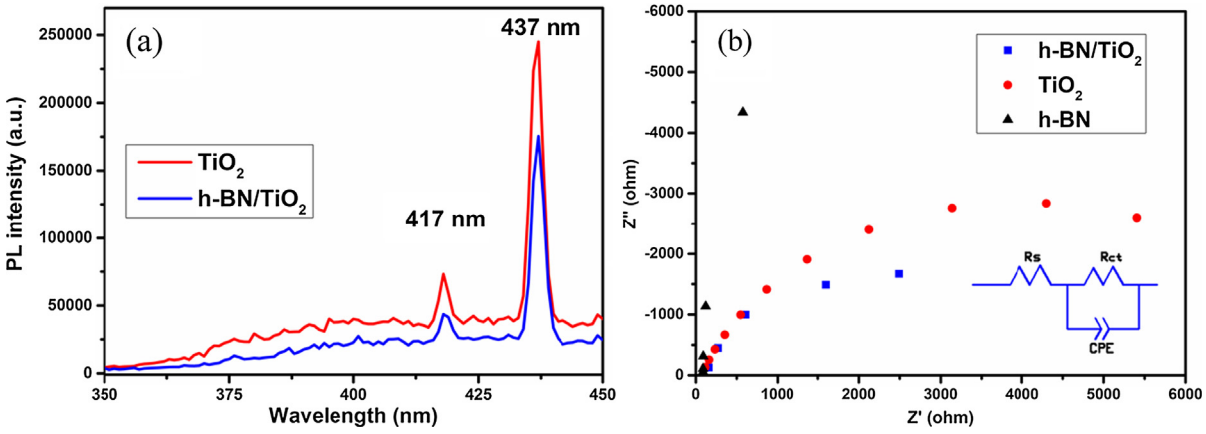

Fig. 7. (a) PL emission spectra of pure TiO_2 nanoparticles and prepared h-BN/TiO_2 nanocomposites, (b) EIS Nyquist spectra of photocatalysts.

(Fig. 5c and d). To be noted, the RhB and MB can be degraded almost completely within 50 min, and the solution color faded to be transparent (inserts of Fig. 5a and c).

Further experiments have been carried out to monitor the kinetics of RhB/MB photocatalytic degradation. It is shown in Fig. 6a and c, with a certain loading of h-BN, the degradation efficiency was enhanced notably for not only RhB but also MB. Compared to pure TiO_2, the h-BN/TiO_2 samples exhibited a higher photocatalytic efficiency. After irradiation for 50 min, the degradation efficiencies reached the highest of 98% and 92% for RhB and MB, respectively. However, the

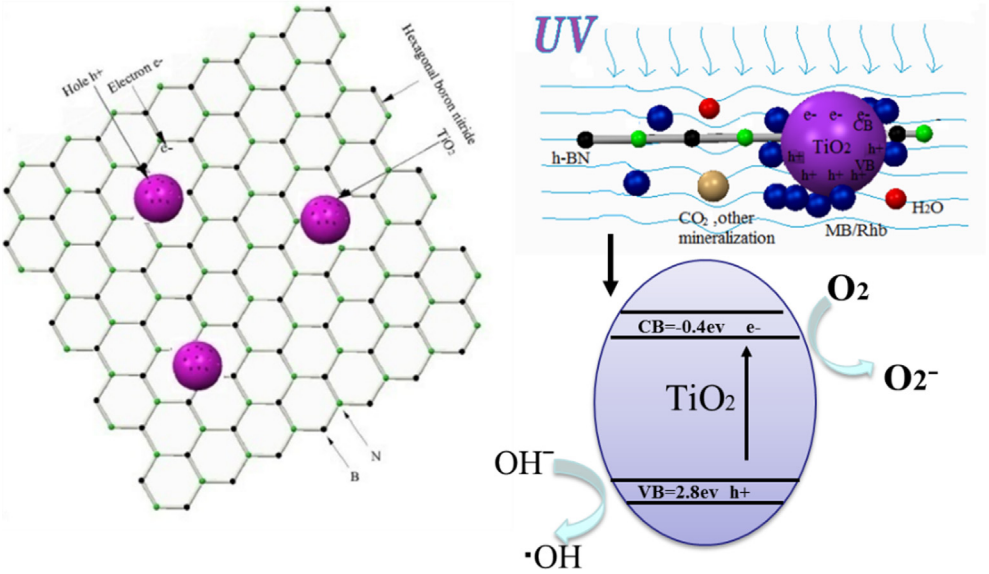

Fig. 8. Schematic photocatalytic mechanism of h-BN/TiO_2 nanocomposites.

corresponding degradation efficiencies were only 54.7% and 56.3% for pure TiO_2. Almost no degradation of dyes was observed over pure h-BN, eliminating the possibility that the absorption of h-BN accounted for the photocatalytic activity. In Fig. 6b and d, it was obvious that the photocatalytic performance of the h-BN/TiO_2 nanocomposites was better than pure h-BN and pure TiO_2. The kinetic data of photocatalytic degradation followed a pseudo-first-order reaction model: $\ln(C/C_0) = -kt$, where C_0 and C are the absorption equilibrium and dye concentrations at reaction time *t*, and *k* is the reaction rate (min^{-1}). The results were displayed in Table 1, the reaction rate *k* (RhB = 0.059518 and MB = 0.0498) of h-BN/TiO_2 nanocomposites for RhB and MB was 3.64 and 4.22 times higher than that of pure TiO_2, respectively. The obtained performance was top in the values of the TiO_2-based photocatalysts, as shown in Table 2.

The stability of h-BN/TiO_2 nanocomposites was evaluated by recycling experiments. As shown in Fig. 6e, after five successive uses, there was only an insignificant degradation efficiency loss for both RhB and MB dyes. And the decreased efficiency can be partially attributed to the drip loss of the samples collection after each cycle. This indicated the good stability and reusability of the h-BN/TiO_2 nanocomposites.

To shed more light on the outstanding performance of h-BN/TiO_2 nanocomposites, the photoluminescence (PL) and the electrochemical impedance spectroscopy (EIS) were carried out. Because the PL emission is caused by the recombination of free carriers, low PL emission intensity indicates a low recombination rate [47,51]. The PL spectra of pure TiO_2 and h-BN/TiO_2 nanocomposites are showed in Fig. 7a. Two emission peaks located at 417 and 437 nm are observed for both pure TiO_2 and h-BN/TiO_2 nanocomposites. It was reported that the emission at 417 nm was attributed to the recombination of electron–hole pair at the band edge of TiO_2 [47], while the emission at 437 nm was related to the recombination at oxygen vacancies [51–53]. The intensities of both emission peaks of the h-BN/TiO_2 nanocomposites were lower than those of pure TiO_2 indicating that the incorporation of h-BN with TiO_2 suppressed the recombination of photogenerated electrons and holes. The EIS was performed to observe the electron transfer kinetics at the interface (Fig. 7b). The fitted Nyquist plots using Z-view software are shown in Fig. 7b. The results accord with Randles equivalent circuit model (inset of Fig. 7b). R_s is the total resistance of the electrolyte solution, R_{ct} and CPE represent the charge transfer resistance across the interface and the capacitance of the space charge region, respectively [54,55]. Generally speaking, the smaller the radii of semicircle arc, the lower the electron-transfer resistance [54]. The arc radius of h-BN/TiO_2 became shorter compared to bare TiO_2 and h-BN, which implied a decrease in the charge transfer resistance at the interface [28,53]. It suggested that h-BN/TiO_2 exhibited the fastest interfacial charge transfer. Meantime, this led to an inhibiting recombination of electrons and holes which was in accordance with the PL response spectrum.

The photocatalytic degradation process for MB and RhB by h-BN/TiO_2 was proposed, as shown in Fig. 8. The TiO_2 nanoparticles are loaded on the h-BN sheet, the electronic transition of the nanocomposites by ultraviolet light produces the photoelectrons and holes. The degradation of dyes is caused by the produced photoelectrons and holes. The formula are shown as follows. During UV irradiation, the photocatalysts were activated to produce photo-generated electrons and holes when the absorbed UV light energy was higher than the energy of the “initial photocatalysts” (formula (2)). Due to the exfoliated h-BN nanosheets containing negative hydroxyls, the photo-generated holes can be easily attracted and reacted with hydroxyls to generate ·OH. Meanwhile, it inhibited the recombination of photo-generated electrons and holes. At the same time, the photo-generated holes can also react with hydroxyls in solution to generate ·OH (Formula (3)). The electrons can react with Ti^{4+} and O_2 to produce O_2^- (Formula (4) and (5)). Dyes were effectively decomposed by ·OH and O_2^- (Formula (6)). In the process, the exfoliated h-BN nanosheets not only provided extra hydroxyls to generate ·OH, but also offered more electrons because once its own hydroxyls reacted with photo-generated holes, the extra photo-generated electrons were free. Finally, the oxidation capacity of the nanocomposites was improved, which resulted in an enhanced photocatalytic degradation of dyes. The processes are summarized as follows:

$$\text{h-BN/TiO}_2 + \text{hv} \rightarrow \text{h-BN/TiO}_2\ (e^- + h^+) \quad (2)$$

$$h^+ + OH^- \rightarrow OH \quad (3)$$

$$Ti^{4+} + e^- \rightarrow Ti^{3+} \quad (4)$$

$$Ti^{3+} + O_2 \rightarrow O_2^- + Ti^{4+} \quad (5)$$

$$\text{Dye} + O_2^- + OH \rightarrow CO_2 + H_2O + OH^- \quad (6)$$

4. Conclusion

In summary, the nanocomposites of h-BN/TiO_2 were prepared via a sol-gel method. TiO_2 served as active photocatalyt and the h-BN sheets played a role of ‘bed’ base. The two-dimensional h-BN sheets with high

specific surface area make TiO_2 nanoparticles dispersed and loaded well on the h-BN sheets. Due to the B—O—Ti bond, the combination between TiO_2 nanoparticles and h-BN sheets was tight. The h-BN/TiO_2 nanocomposites exhibited excellent photocatalytic efficiency, the degradation efficiencies of RhB and MB reached 98% and 92%, respectively. Besides, the nanocomposite photocatalysts were quite stable and recoverable. The enhanced photocatalytic performance of the nanocomposites was reasonably attributed to the fact that the transfer rate of photogenerated electrons is accelerated and the recombination efficiency of photogenerated charges is decreased.

Acknowledgement

We greatly acknowledge the funding for this project through the Priority Academic Program Development of Jiangsu Higher Education Institution; the Key Laboratory is funded by Jiangsu advanced welding technology; National Natural Science Foundation of China (51873083, 21301072), Six Talent Peaks Project in Jiangsu Province, China (No. 2015-XCL-028) and Postgraduate Research & Practice Innovation Program of Jiangsu Province (KYCX17-1831).

Appendix A. Supplementary material

Supplementary data to this article can be found online at https://doi.org/10.1016/j.apsusc.2018.09.137.

References

[1] D. Chatterjee, S. Dasgupta, Visible light induced photocatalytic degradation of organic pollutants, J. Photochem. Photobiol. C: Photochem. Rev. 6 (2005) 186–205.
[2] U.I. Gaya, A.H. Abdullah, Heterogeneous photocatalytic degradation of organic contaminants over titanium dioxide: a review of fundamentals, progress and problems, J. Photochem. Photobiol. C: Photochem. Rev. 9 (2008) 1–12.
[3] X. Chen, S. Shen, L. Guo, S.S. Mao, Semiconductor-based photocatalytic hydrogen generation, Chem. Rev. 110 (2010) 6503–6570.
[4] D.Y.C. Leung, X. Fu, C. Wang, M. Ni, M.K.H. Leung, X. Wang, X. Fu, Hydrogen production over titania-based photocatalysts, Chem. Sus. Chem. 3 (2010) 681–694.
[5] H. Lin, C. Huang, W. Li, C. Ni, S. Shah, Y. Tseng, Size dependency of nanocrystalline TiO_2 on its optical property and photocatalytic reactivity exemplified by 2-chlorophenol, Appl. Catal. B: Environ. 68 (2006) 1–11.
[6] J. Zhang, Q. Xu, Z. Feng, M. Li, C. Li, Importance of the relationship between surface phases and photocatalytic activity of TiO_2, Angew. Chem. Int. Ed. 47 (2008) 1766–1769.
[7] X. Han, Q. Kuang, M. Jin, Z. Xie, L. Zheng, Synthesis of titania nanosheets with a high percentage of exposed (001) facets and related photocatalytic properties, J. Am. Chem. Soc. 131 (2009) 3152–3153.
[8] X.-Y. Zhang, H.-P. Li, X.-L. Cui, Y. Lin, Graphene/TiO_2 nanocomposites: synthesis, characterization and application in hydrogen evolution from water photocatalytic splitting, J. Mater. Chem. 20 (2010) 2801.
[9] J. Zhang, J.H. Bang, C. Tang, P.V. Kamat, Tailored $TiO_2-SrTiO_3$ heterostructure nanotube arrays for improved photoelectrochemical performance, ACS Nano 4 (2010) 387–395.
[10] K. Woan, G. Pyrgiotakis, W. Sigmund, Photocatalytic carbon-nanotube–tio$_2$ composites, Adv. Mater. 21 (2009) 2233–2239.
[11] A.L. Linsebigler, G. Lu, J.T. Yates, Photocatalysis on TiO_2 surfaces: principles, mechanisms, and selected results, Chem. Rev. 95 (1995) 735–758.
[12] K.M. Schindler, M. Kunst, Charge-carrier dynamics in titania powders, J. Phys. Chem. 94 (1990) 8222–8226.
[13] P.V. Kamat, Photochemistry on nonreactive and reactive (semiconductor) surfaces, Chem. Rev. 93 (1993) 267–300.
[14] M.R. Hoffmann, S.T. Martin, W. Choi, D.W. Bahnemann, Environmental applications of semiconductor photocatalysis, Chem. Rev. 95 (1995) 69–96.
[15] H.G. Yang, C.H. Sun, S.Z. Qiao, J. Zou, G. Liu, S.C. Smith, H.M. Cheng, G.Q. Lu, Anatase TiO_2 single crystals with a large percentage of reactive facets, Nature 453 (2008) 638–641.
[16] N. Serpone, P. Maruthamuthu, P. Pichat, E. Pelizzetti, H. Hidaka, Exploiting the interparticle electron transfer process in the photocatalysed oxidation of phenol, 2-chlorophenol and pentachlorophenol: chemical evidence for electron and hole transfer between coupled semiconductors, J. Photochem. Photobiol. A: Chem. 85 (1995) 247–255.
[17] X. Fu, Y. Hu, T. Zhang, S. Chen, The role of ball milled h-BN in the enhanced photocatalytic activity: a study based on the model of ZnO, Appl. Surf. Sci. 280 (2013) 828–835.
[18] K. Siwińska-Stefańska, B. Kurc, Preparation and application of a titanium dioxide/graphene oxide anode material for lithium–ion batteries, J. Power Sources 299 (2015) 286–292.
[19] H.A.R.A. Hussian, M.A.M. Hassan, I.R.A. gool, Synthesis of titanium dioxide (TiO_2) nanofiber and nanotube using different chemical method, Optik – Int. J. Light Elect. Opt. 127 (2016) 2996–2999.
[20] H. Lv, Y. Liu, H. Tang, Synergetic effect of MoS_2 and graphene as cocatalysts for enhanced photocatalytic activity of $BiPO_4$ nanoparticles, Appl. Surf. Sci. 425 (2017) 100–106.
[21] W. Teng, Y. Wang, H. Huang, Enhanced photoelectrochemical performance of MoS_2 nanobelts-loaded TiO_2 nanotube arrays by photo-assisted electrodeposition, Appl. Surf. Sci. 425 (2017) 507–517.
[22] L. Valentini, M. Cardinali, S. Bittolo Bon, D. Bagnis, R. Verdejo, M.A. Lopez-Manchado, J.M. Kenny, Use of butylamine modified graphene sheets in polymer solar cells, J. Mater. Chem. 20 (2010) 995–1000.
[23] A. Nag, K. Raidongia, K.P.S.S. Hembram, R. Datta, U.V. Waghmare, C.N.R. Rao, Graphene analogues of BN: novel synthesis and properties, ACS Nano 4 (2010) 1539–1544.
[24] Y. Lin, T.V. Williams, T.-B. Xu, W. Cao, H.E. Elsayed-Ali, J.W. Connell, Aqueous dispersions of few-layered and monolayered hexagonal boron nitride nanosheets from sonication-assisted hydrolysis: critical role of water, J. Phys. Chem. C 115 (2011) 2679–2685.
[25] D.-H. Cho, J.-S. Kim, S.-H. Kwon, C. Lee, Y.-Z. Lee, Evaluation of hexagonal boron nitride nano-sheets as a lubricant additive in water, Wear 302 (2013) 981–986.
[26] C. Huang, W. Ye, Q. Liu, X. Qiu, Dispersed Cu_2O Octahedrons on h-BN Nanosheets for p-Nitrophenol Reduction, ACS Appl. Mater. Interf. 6 (2014) 14469–14476.
[27] J.N. Coleman, M. Lotya, A. O'Neill, S.D. Bergin, P.J. King, U. Khan, K. Young, A. Gaucher, S. De, R.J. Smith, I.V. Shvets, S.K. Arora, G. Stanton, H.Y. Kim, K. Lee, G.T. Kim, G.S. Duesberg, T. Hallam, J.J. Boland, J.J. Wang, J.F. Donegan, J.C. Grunlan, G. Moriarty, A. Shmeliov, R.J. Nicholls, J.M. Perkins, E.M. Grieveson, K. Theuwissen, D.W. McComb, P.D. Nellist, V. Nicolosi, Two-dimensional nanosheets produced by liquid exfoliation of layered materials, Science 331 (2011) 568–571.
[28] Y. Gu, M. Xing, J. Zhang, Synthesis and photocatalytic activity of graphene based doped TiO_2 nanocomposites, Appl. Surf. Sci. 319 (2014) 8–15.
[29] X. Pan, Y. Zhao, S. Liu, C.L. Korzeniewski, S. Wang, Z. Fan, Comparing graphene-TiO_2 nanowire and graphene-TiO_2 nanoparticle composite photocatalysts, ACS Appl. Mater. Interf. 4 (2012) 3944–3950.
[30] V. Štengl, J. Henych, M. Slušná, h-BN-TiO_2 nanocomposite for photocatalytic applications, J. Nanomater. 2016 (2016) 1–12.
[31] W.F. Zhang, Y.L. He, M.S. Zhang, Z. Yin, Q. Chen, Raman scattering study on anatase TiO_2 nanocrystals, J. Phys. D Appl. Phys. 33 (2000) 912.
[32] S.D. Perera, R.G. Mariano, K. Vu, N. Nour, O. Seitz, Y. Chabal, K.J. Balkus, Hydrothermal synthesis of graphene-TiO_2 nanotube composites with enhanced photocatalytic activity, ACS Catal. 2 (2012) 949–956.
[33] E. Bilgin Simsek, Solvothermal synthesized boron doped TiO_2 catalysts: Photocatalytic degradation of endocrine disrupting compounds and pharmaceuticals under visible light irradiation, Appl. Catal. B 200 (2017) 309–322.
[34] H. Jung, K. Nam, H.-G. Sung, H. Hyun, Y. Sohn, W. Shin, Preparation of TiO_2-decorated boron particles by wet ball milling and their photoelectrochemical hydrogen and oxygen evolution reactions, Materials 9 (2016) 1012.
[35] T. Sainsbury, A. Satti, P. May, Z. Wang, I. McGovern, Y.K. Gun'ko, J. Coleman, Oxygen radical functionalization of boron nitride nanosheets, J. Am. Chem. Soc. 134 (2012) 18758–18771.
[36] D.H. Quiñones, A. Rey, P.M.Á. lvarez, F.J. Beltrán, G.L. i Puma, Boron doped TiO2 catalysts for photocatalytic ozonation of aqueous mixtures of common pesticides: Diuron, o-phenylphenol, MCPA and terbuthylazine, Appl. Catal. B 178 (2015) 74–81.
[37] B.J. Kim, H. Jang, S.-K. Lee, B.H. Hong, J.-H. Ahn, J.H. Cho, High-performance flexible graphene field effect transistors with ion gel gate dielectrics, Nano Lett. 10 (2010) 3464–3466.
[38] Y. Liu, Y. Zhou, L. Yang, Y. Wang, Y. Wu, C. Li, J. Lu, Hydrothermal synthesis of 3D urchin-like Ag/TiO_2/reduced graphene oxide composites and its enhanced photocatalytic performance, J. Nanopart. Res. 18 (2016) 283.
[39] J.H. Chen, M. Ishigami, C. Jang, D.R. Hines, M.S. Fuhrer, E.D. Williams, Printed graphene circuits, Adv. Mater. 19 (2007) 3623–3627.
[40] B. Buchholcz, E. Varga, T. Varga, K. Plank, J. Kiss, Z. Kónya, Structure and stability of boron doped titanate nanotubes and nanowires, Vacuum 138 (2017) 120–124.
[41] A. Ismach, H. Chou, D.A. Ferrer, Y. Wu, R.S. Ruoff, Toward the controlled synthesis of hexagonal boron nitride films, ACS Nano 6 (2012) 6378–6385.
[42] C. Hou, Q. Zhang, Y. Li, H. Wang, P25-graphene hydrogels: room-temperature synthesis and application for removal of methylene blue from aqueous solution, J. Hazard. Mater. 205–206 (2012) 229–235.
[43] C. Xu, P. Chen, J. Liu, H. Yin, X. Gao, X. Mei, Fabrication of visible-light-driven Ag/TiO_2 heterojunction composites induced by shock wave, J. Alloy. Compd. 679 (2016) 463–469.
[44] S. Filice, D. D'Angelo, S. Libertino, I. Nicotera, V. Kosma, V. Privitera, S. Scalese, Graphene oxide and titania hybrid Nafion membranes for efficient removal of methyl orange dye from water, Carbon 82 (2015) 489–499.
[45] B.Y.S. Chang, M.S. Mehmood, A. Pandikumar, N.M. Huang, H.N. Lim, A.R. Marlinda, N. Yusoff, W.S. Chiu, Hydrothermally prepared graphene-titania nanocomposite for the solar photocatalytic degradation of methylene blue, Desalin. Water Treat. 57 (2016) 238–245.
[46] J. Wang, J. Shen, D. Fan, Z. Cui, X. Lü, J. Xie, M. Chen, BN nanosheet: an efficient carriers transfer promoter and stabilizer to enhance the photocatalytic performance of Ag_2CO_3, Mater. Lett. 147 (2015) 8–11.
[47] X. Fu, Y. Hu, Y. Yang, W. Liu, S. Chen, Ball milled h-BN: an efficient holes transfer promoter to enhance the photocatalytic performance of TiO_2, J. Hazard. Mater. 244–245 (2013) 102–110.
[48] S. Gayathri, M. Kottaisamy, V. Ramakrishnan, Facile microwave-assisted synthesis

of titanium dioxide decorated graphene nanocomposite for photodegradation of organic dyes, AIP Adv. 5 (2015) 127219.
[49] J. Hu, H. Li, Q. Wu, Y. Zhao, Q. Jiao, Synthesis of TiO2 nanowire/reduced graphene oxide nanocomposites and their photocatalytic performances, Chem. Eng. J. 263 (2015) 144–150.
[50] X. Qin, L. Jing, G. Tian, Y. Qu, Y. Feng, Enhanced photocatalytic activity for degrading Rhodamine B solution of commercial Degussa P25 TiO_2 and its mechanisms, J. Hazard. Mater. 172 (2009) 1168–1174.
[51] J. Liqiang, F. Honggang, W. Baiqi, W. Dejun, X. Baifu, L. Shudan, S. Jiazhong, Effects of Sn dopant on the photoinduced charge property and photocatalytic activity of TiO_2 nanoparticles, Appl. Catal. B 62 (2006) 282–291.
[52] K. Dong, J. He, J. Liu, F. Li, L. Yu, Y. Zhang, X. Zhou, H. Ma, Photocatalytic performance of Cu_2O-loaded TiO_2/rGO nanoheterojunctions obtained by UV reduction, J. Mater. Sci. 52 (2017) 6754–6766.
[53] J.-G. Yu, H.-G. Yu, B. Cheng, X.-J. Zhao, J.C. Yu, W.-K. Ho, The effect of calcination temperature on the surface microstructure and photocatalytic activity of TiO_2 thin films prepared by liquid phase deposition, J. Phys. Chem. B 107 (2003) 13871–13879.
[54] J. Li, N. Lei, L. Guo, Q. Song, Z. Liang, Constructing h-BN/Bi_2WO_6 quantum dot hybrid with fast charge separation and enhanced photoelectrochemical performance by using h-BN for hole transfer, Chem. Electro. Chem. 5 (2018) 300–308.
[55] X. Chang, T. Wang, P. Zhang, J. Zhang, A. Li, J. Gong, Enhanced surface reaction kinetics and charge separation of p–n heterojunction Co_3O_4/$BiVO_4$ photoanodes, J. Am. Chem. Soc. 137 (2015) 8356–8359.